SCIENTIFIC REPORTS

OPEN

SUBJECT AREAS:
PHYSIOLOGY
BIOPHYSICS
BIOENERGETICS

Received
17 March 2014

Accepted
19 May 2014

Published
9 June 2014

Correspondence and requests for materials should be addressed to P.P. (prodromos.parasoglou@nyumc.org)

Three-dimensional Saturation Transfer ^{31}P-MRI in Muscles of the Lower Leg at 3.0 T

Prodromos Parasoglou, Ding Xia, Gregory Chang & Ravinder R. Regatte

Quantitative Multinuclear Musculoskeletal Imaging Group (QMMIG), Department of Radiology, Center for Biomedical Imaging, New York University Langone Medical Center, New York, NY, USA.

The creatine kinase (CK) reaction plays a critical role in skeletal muscle function, and can be studied non-invasively using phosphorus (^{31}P) saturation transfer (ST) techniques. However, due to the low MR sensitivity of the ^{31}P nucleus, most studies on clinically approved magnetic fields (≤3.0 T) have been performed with coarse resolution and limited tissue coverage. However, such methods are not able to detect spatially resolved metabolic heterogeneities, which may be important in diseases of the skeletal muscle. In this study, our aim was to develop and implement a ^{31}P-MRI method for mapping the kinetics of the CK reaction, and the unidirectional phosphocreatine (PCr) to adenosine triphosphate (ATP) metabolic fluxes in muscles of the lower leg on a clinical 3.0 T MR scanner. We imaged the lower leg muscles of ten healthy volunteers (total experimental time: 40 min, nominal voxel sizes 0.5 mL), and found statistically significant differences between the kinetics of the CK reaction among muscle groups. Our developed technique may allow in the future the early detection of focal metabolic abnormalities in diseases that affect the function of the skeletal muscle.

Phosphorus (^{31}P) magnetic resonance (MR) is a unique non-invasive tool for studying muscle physiology, and has been used extensively for studying diseases that adversely affect muscle function, such as heart failure[1], stroke, congenital myopathies[2], and ischemic heart disease[3]. A unique feature of saturation transfer (ST) ^{31}P-MR techniques is their ability to measure the kinetics of important metabolic reactions that involve phosphorus containing metabolites[4]. High-energy phosphate is reversibly transferred between adenosine triphosphate (ATP) and phosphocreatine (PCr) through the creatine kinase (CK) reaction. Disturbances in the kinetics of the CK reaction are found in many disease that affect myocardial energy metabolism[5,6]. However, in the skeletal muscle the physiological significance of alterations on the CK exchange rate are less understood.

The kinetics of the CK reaction have been studied extensively using surface radiofrequency (RF) coils and, either unlocalized[7] or localized methods with limited tissue coverage[8]. However, such methods lack the ability to measure muscle-specific energy metabolism and therefore cannot identify potential heterogeneneities in muscle function in health and disease. The development of relatively high-resolution and large tissue coverage imaging approaches for identifying spatial heterogeneities in the kinetics of the CK reaction may enable a better understanding of the CK role in the muscle.

A major roadblock for the development of high-resolution ^{31}P-MR methods with sufficient tissue coverage is the low MR sensitivity of the ^{31}P nucleus and the relatively low concentration of ^{31}P containing metabolites in the human tissue. The increased availability of ultra-high field (UHF) whole body magnets (≥7.0 T) has allowed the development of time efficient ^{31}P-MR methods that provide adequate tissue coverage and significantly increased spatial resolution[9–11]. However, only a few tens of UHF systems are currently operational worldwide[12], while most of the clinical MRI work is performed almost exclusively in fields of 3.0 T or lower. Therefore, it is equally important to develop ^{31}P-MR tools for the diagnosis of complications in the skeletal muscle in fields of 3.0 T or lower.

In this study, we aimed at developing and implementing a three-dimensional saturation transfer (ST) ^{31}P-MRI method capable of mapping the CK reactions kinetics in the entire muscle of the lower leg on a clinically approved 3.0 T whole body magnet. Our method maps the unidirectional conversion rate of PCr-to-ATP at relatively high spatial resolution (i.e. 0.5 mL voxel size), in a total acquisition time of 40 min, and can potentially be used in a routine clinical setting.

Results

In order to estimate the pseudo first-order forward rate constant (k_f) of the CK reaction, we need to measure the phosphocreatine (PCr) signal while we saturate the γ-adenosine triphosphate (γ-ATP) resonance for different

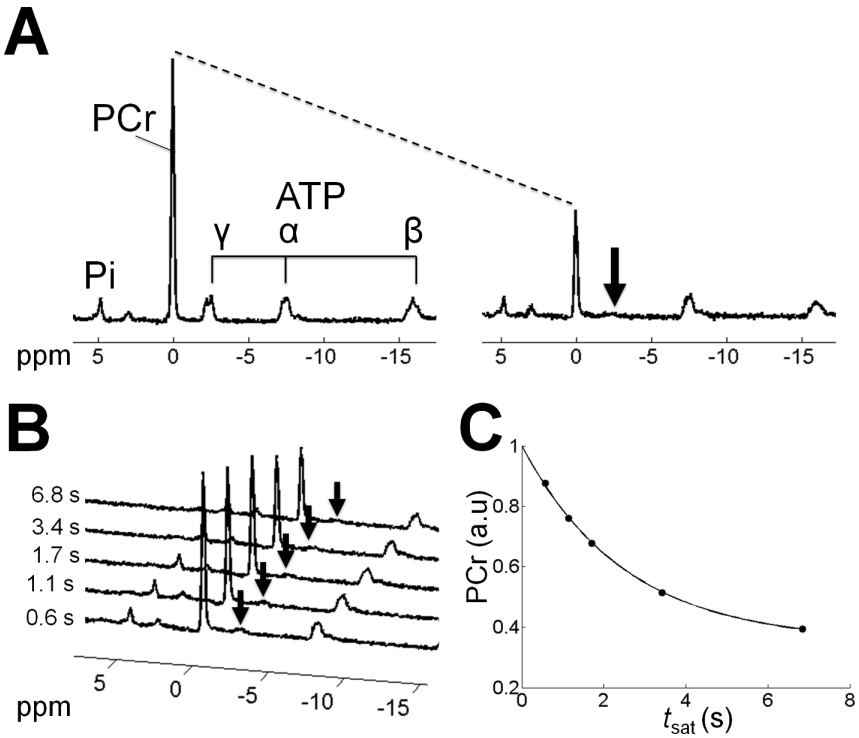

Figure 1 | Unlocalized ST-^{31}P-MRS of the lower leg. A) Fully relaxed ^{31}P spectrum without ST preparation (t_{sat} = 0 s) (left) and ^{31}P-ST Spectrum with complete saturation (arrow) of the γ-ATP resonance (t_{sat} = 6.84 s) (right). B) Series of ST spectra at different t_{sat}. C) PCr signal intensity fitted to Eq.2, (Pearson's product moment correlation = 0.9992).

durations (i.e. the progressive ST experiment)[13]. Assuming a two-pool exchange system between PCr and γ-ATP and complete saturation of γ-ATP, we can estimate the exchange rate between the two metabolites by solving the modified, for chemical exchange, Bloch equation[14] (see methods). To confirm the efficiency of our saturation pulses, we acquired unlocalized ^{31}P spectra in the entire volume of the lower leg muscles in all of our volunteers. Typical ^{31}P spectra can be seen in Fig. 1, where the full width at half maximum of the PCr resonance peak was 12.3 ± 4.8 Hz (mean ± SD) across all subjects. As we show in the same figure, the ST module saturates γ-ATP to levels not measurable above the noise.

Fat infiltration, especially in high body mass index (BMI) subjects, can reduce the volume fraction of lean muscle in a certain volume of tissue affecting quantification of PCr concentration. In order to account for the fat content in the muscle, the Hierarchical IDEAL method[15] was applied across all subjects. The fat volume fractions in the TA were 0.035 ± 0.006 across all subjects, significantly lower than in the GL (0.056 ± 0.019, $P = 0.012$), the GM (0.051 ± 0.020, $P < 0.001$) and the S (0.063 ± 0.020, $P = 0.002$) muscles. Figure 2 shows a case of a higher BMI (30.4) subject. The water/fat separation method shows fat infiltration in the leg muscles. The fat volume fraction in the GM was 0.11, and 0.04 in the TA, which, if not accounted for (especially the GM), can lead to under-estimation of the PCr concentration.

In the turbo spin echo (TSE) imaging method, the echo amplitude is modulated as a function of the echo position in *k*-space, resulting in blurring[16]. We estimated the point spread function (PSF) of our imaging method as the result of the echo modulation to be at 1.6 pixels in the anterior to posterior direction, where the echo train is sampled.

Figure 3A shows an anatomical cross-section of the lower leg muscles of a lean subject (BMI = 19.5) and a cross-section of the PCr concentration map (Fig. 3B). PCr in the same cross-section decreases with increasing saturation time (t_{sat}) as shown in Fig. 3C. By segmenting signals in the PCr images and fitting data to Eq.2 (methods), we estimated k_f and the unidirectional flux of PCr to form ATP (V_f) for four muscle groups of the leg [Gastrocnemius Lateralis (GL) and Medialis (GM), Soleus (S), and Tibialis Anterior (TA)]. We estimated the intrinsic spin lattice relaxation (T_1') in the presence of saturating irradiation[17] from Eq.3. The results are summarized in Table 1. In the TA, k_f was significantly lower than the GL ($P = 0.002$), the GM ($P = 0.029$) and the S ($P = 0.037$). The metabolic fluxes, V_f, in the TA were lower than both the GL ($P < 0.001$) and the GM ($P = 0.043$). We did not find any statistically significant differences among T_1' values in the four muscle groups.

Discussion

Our study focused on the development and implementation of a ST-^{31}P-MRI method capable of obtaining muscle specific measurements of the CK reaction and metabolic fluxes of PCr to ATP in the entire volume of the muscles of the lower leg using a clinical high-field (3.0 T) scanner. Our method enables such measurements with relatively high spatial resolution (i.e. 0.5 mL voxel size) and large muscle coverage within an acquisition time of 40 min.

Our imaging approach (Fig. 4B) is based on a fast 3D-TSE sequence, which excites and acquires a single resonance of the ^{31}P-MR spectrum

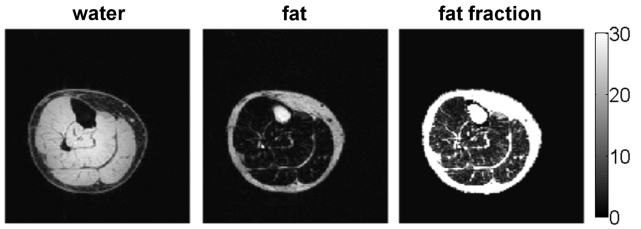

Figure 2 | Water/fat fractions in the lower leg. The water (left) and fat (right) images of a subject (BMI = 30.4) are shown. The fat fraction (right) shows fat infiltration in the leg muscles.

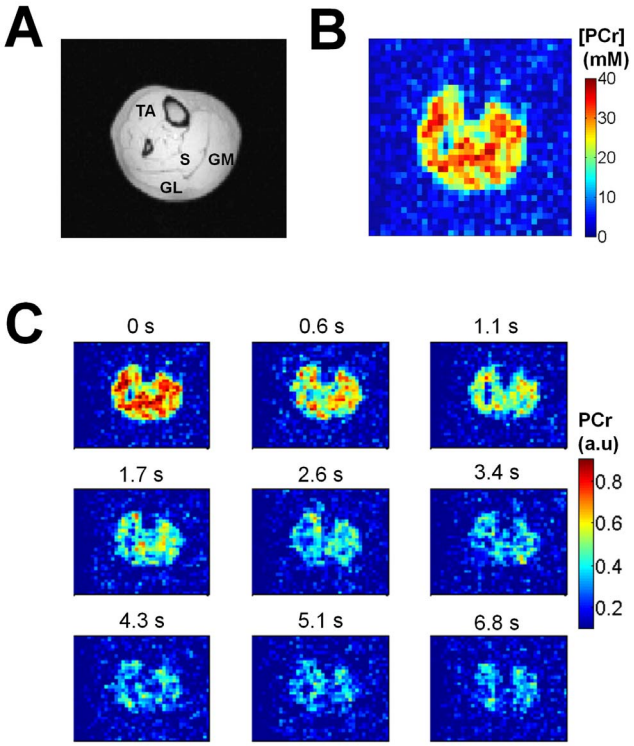

Figure 3 | Saturation transfer ^{31}P-MRI. A) Anatomical proton image where four major muscle groups are identified. B) PCr concentration map in a cross-section of the lower leg. C) ST-^{31}P-MRI of the same cross-section at different saturation times. PCr signal intensity decreases as the system is allowed to exchange for longer time.

(i.e. PCr). By trading spectral information for imaging speed, we are able to accelerate acquisition time and increase spatial resolution compared to ^{31}P-MRS[18,19] approaches, while obtaining full coverage of the muscle. As shown in Eq.2, estimation of k_f only requires measurement of PCr signal at different saturation times.

Our results are in close agreement with previous ^{31}P-MR studies. Valkovic *et al.*[7], measured a mean k_f in the Gastrocnemius muscle at 0.31 s^{-1} both at 3.0 T and 7.0 T, using unlocalized ^{31}P-MRS. Our mean measured k_f in the GL was 0.32 s^{-1} (Table 1) and 0.31 s^{-1} in the GM. In an earlier study, Bottomley *et al.*[20] reported a mean k_f of 0.27 s^{-1} using a localized MRS method at 1.5 T. Our measurements of PCr concentration are well within the range reported in several studies reviewed by Kemp *et al.*[21]. As seen in Table 1, our measurements showed significant lower k_f in the TA compared to the other three muscle groups (i.e. GL, GM, S). These results agree with the values we reported at UHF[22], using ^{31}P-MRI. To the best of our knowledge, no ST studies using spectroscopy have been reported for that particular muscle. In terms of our T_1' measurements, Schar *et al.*[8] reported mean values of 2.27 s in the calf muscle at 3.0 T, which is very close to the mean reported values in our work for the GL (2.11 s) and the GM (2.15 s).

The main limitation of our spectrally selective imaging approach, compared to ^{31}P-MRS methods, is the lack of localized measurements of ATP, which may have a two-fold effect in quantifying k_f and V_f. First, in the ST experiments, there could be remaining γ-ATP signal that is not fully suppressed. If that is the case, there could be local errors in the estimation of k_f that are not accounted for by Eq.2. However, unlocalized ^{31}P-MRS measurements in the entire volume of the lower leg muscles (Fig. 1) did not show any evidence of unsuppressed γ-ATP signal, hence we do not expect that this would affect quantification in our study. Second, ^{31}P-MRS studies assume constant ATP concentration in the skeletal muscle[21], and estimate PCr concentration from the ratio of the PCr signal to that of ATP. Our study requires the use of external phantoms and in some cases (i.e. high BMI subjects) water-content corrections that complicate the process of quantifying resting PCr concentration.

Of note, our imaging method could also be translated for studying metabolic activity in the brain. The CK reaction rate has been studied with one-dimensional spectroscopy[23] at 3.0 T, while our method could provide full-coverage of the brain in similar acquisition time.

Compared to UHF, ^{31}P MRI at 3.0 T suffers from a close to three-fold decreased signal to noise ratio[24]. In our implementation at UHF[22], we used a constant saturation time prior to imaging, and measured T_1' in a separate experiment. However, at 3.0 T, we found that mapping T_1' was particularly challenging, with the images acquired at different inversion times not yielding sufficient SNR in order to have accurate fittings of the recovery curve. In the work presented here, we used the progressive saturation approach, where we saturate γ-ATP for different durations. Through a three-parameter fitting of Eq.2 to the data, we recovered T_1 and k_f for each muscle which was then used in Eq.3 to estimate T_1'. In this approach,

Table 1 | Results of the ST experiments in four major leg muscles. Asterisks depict statistically significant differences between muscle groups ($P < 0.05$)

	TA				GL				GM				S			
Vol.	k_f	T_1'	[PCr]	V_f	k_f	T_1'	[PCr]	V_f	k_f	T_1'	[PCr]	V_f	k_f	T_1'	[PCr]	V_f
#	(s^{-1})	(s)	(mM)	(mM s^{-1})	(s^{-1})	(s)	(mM)	(mM s^{-1})	(s^{-1})	(s)	(mM)	(mM s^{-1})	(s^{-1})	(s)	(mM)	(mM s^{-1})
1	0.29	2.11	33.65	9.74	0.29	2.48	33.96	9.90	0.35	2.00	36.10	12.53	0.37	1.83	33.42	12.31
2	0.16	4.12	36.60	5.91	0.26	2.29	36.31	9.50	0.30	2.23	37.40	11.33	0.30	1.99	32.81	9.75
3	0.25	2.41	29.57	7.28	0.27	2.68	32.61	8.89	0.30	1.94	29.96	9.03	0.26	2.57	27.67	7.16
4	0.28	2.05	34.27	9.48	0.34	1.88	35.47	11.95	0.29	2.26	34.43	9.97	0.26	2.50	31.75	8.37
5	0.26	2.42	31.12	8.03	0.27	2.74	32.91	8.76	0.25	2.77	32.90	8.18	0.29	2.45	30.37	8.82
6	0.25	2.27	33.54	8.47	0.30	2.21	34.49	10.26	0.23	2.84	33.76	7.71	0.28	2.24	31.66	9.02
7	0.23	2.51	31.77	7.20	0.30	1.82	29.00	8.84	0.30	2.11	30.35	8.96	0.27	2.09	28.26	7.67
8	0.34	1.69	34.22	11.52	0.37	1.50	33.22	12.40	0.32	1.80	32.92	10.65	0.30	2.03	35.17	10.71
9	0.30	1.88	29.22	8.90	0.42	1.64	28.84	12.06	0.36	1.81	27.83	9.89	0.39	1.73	26.50	10.30
10	0.27	2.16	30.85	8.29	0.32	2.00	27.93	9.56	0.37	1.72	28.09	10.44	0.32	2.00	27.31	8.63
avg	**0.26***	**2.39**	**32.48**	**8.48****	**0.32**	**2.11**	**32.48**	**10.21**	**0.31**	**2.15**	**32.37**	**9.87**	**0.30**	**2.14**	**30.49**	**9.27**
SD	**0.05**	**0.66**	**2.35**	**1.56**	**0.05**	**0.44**	**2.92**	**1.41**	**0.05**	**0.39**	**3.25**	**1.16**	**0.04**	**0.29**	**2.94**	**1.53**

*significantly lower than GL, GM, S.
**significantly lower than GL, GM.

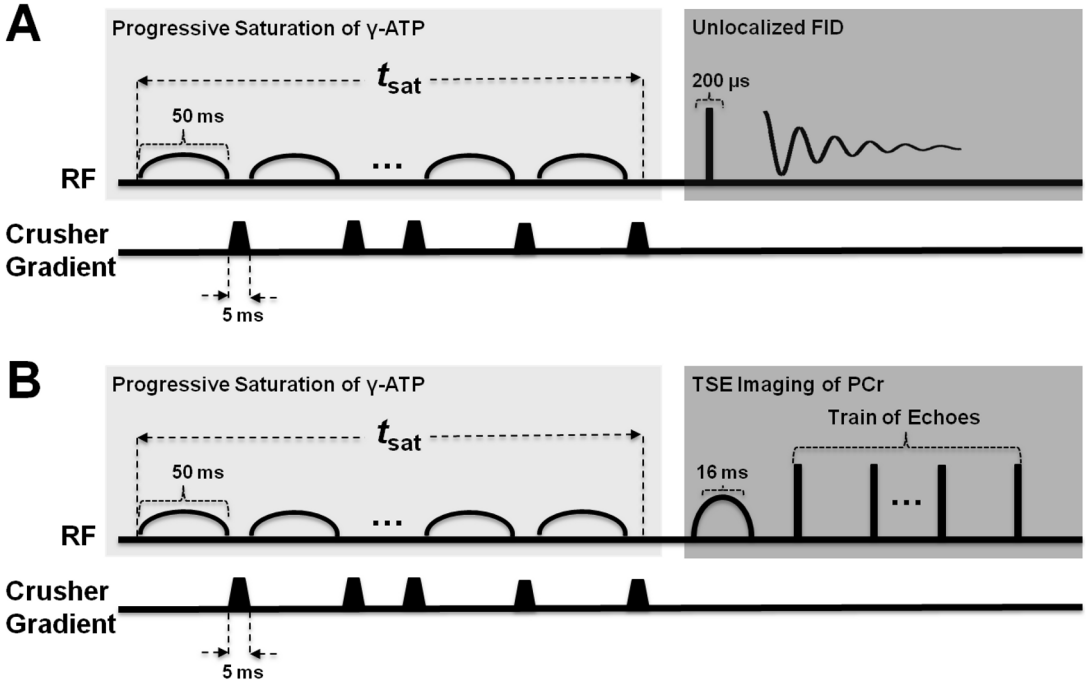

Figure 4 | Saturation transfer spectroscopy (ST-^{31}P-MRS) and imaging (ST-^{31}P-MRI) pulse sequences. A saturation transfer module consists of a train of Gaussian pulses, which saturates the γ-ATP resonance. Spoiler gradients are used between two consecutive pulses to destroy any remaining transverse magnetization. The number of Gaussian pulses defines t_{sat} in each experiment. A) Unlocalized ^{31}PMRS data were acquired by sampling the free induction decay (FID) after implementing the ST module. B) Identical ST preparation module as in ^{31}P-MRS, followed by a spectrally selective ^{31}P-MRI imaging sequence.

the PCr signal for all t_{sat} is between 40–100% of the reference signal (Fig. 1), allowing for accurate fitting of Eq.2 to the data.

In summary, ^{31}P-MR is unique in its ability to non-invasively probe human metabolism in vivo. High-field (3.0 T) clinical magnets provide sufficient sensitivity in order to perform imaging experiments with large tissue coverage and relatively high spatial resolution for measuring muscle-specific energy metabolism in the skeletal muscle and potential disruptions in local energy metabolism caused by disease.

Methods

Theory. The CK reaction can be written as:

$$PCr + ADP + H^{+} \underset{k_r}{\overset{k_f}{\leftrightarrow}} ATP + Cr \quad (1)$$

with k_f and k_r the pseudo first-order forward and reverse rate constants respectively[4]. One approach for measuring k_f is to saturate the γ-ATP resonance for different durations (the progressive ST experiment)[13]. The saturated magnetization of γ-ATP is transferred to PCr (Eq.1), resulting in a net decrease of the PCr signal. The forward rate k_f can be calculated from the relative decrease of the PCr signal as a function of saturation time (t_{sat}). The CK rate constant k_f multiplied by the PCr concentration yields the unidirectional flux of PCr to form ATP. Under fully-relaxed conditions, assuming complete saturation of the γ-ATP resonance, the magnetization of PCr as a function of t_{sat} can be derived from the solution of the Bloch equations, modified for chemical exchange (assuming a two-pool exchange system)[14]:

$$M(t_{sat}) = c\left[1 + k_f T_1 e^{-(\frac{1}{T_1} + k_f)t_{sat}}\right] \quad (2)$$

Where $M(t_{sat})$ the magnitude of the PCr signal measured at different times (t_{sat}), c a parameter accounting for direct spill-over effects (i.e. direct saturation of PCr by saturating irradiation on γ-ATP), and T_1 the spin-lattice relaxation time of PCr. By measuring the PCr signal for several t_{sat}, k_f can be estimated through a three-parameter (i.e. c, k_f and T_1) fit of the data to Eq.2.

The intrinsic spin lattice relaxation (T_1') in the presence of saturating irradiation is[17]:

$$\frac{1}{T_1'} = \frac{1}{T_1} + k_f \quad (3)$$

Human Subjects. The study was fully Health Insurance Portability and Accountability Act (HIPAA)–compliant and approved by the NYU Institutional Review Board. We obtained written informed consent from all participants in this study. The methods were carried out in accordance with Food and Drugs Administration (FDA) guidelines. We recruited ten non-smoking healthy volunteers (seven men, three women, 32.0 ± 3.5 years of age, range 29–41, BMI 22.6 ± 3.9, range 18.5–30.4) without any medical history of disease affecting muscle function or blood flow. We imaged them on a 3.0 T MRI system (Tim Trio, Siemens Medical Solutions, Erlangen, Germany) using a dual-tuned (^{31}P/^{1}H) transmit-receive quadrature birdcage knee coil (Rapid MRI, Ohio) (18 cm inner diameter).

^{31}P-ST Spectroscopy and Imaging. We performed shimming on the entire volume of the lower leg muscles, using the proton channel of the dual-tuned coil and an iterative shimming algorithm provided by the manufacturer. We acquired ST spectroscopy and imaging data using the pulse sequences shown in Fig. 4.

Equation 2 holds for complete saturation of γ-ATP[14]. To confirm the efficiency of our ST module to saturate γ-ATP, we tested it using an unlocalized pulse acquire sequence (Fig. 4A). Acquisition parameters of the sequence are summarized in Table 2. We zero-filled data to 8-k data points prior to reconstruction, and applied baseline correction for each spectrum separately.

We acquired ST imaging data using the progressive saturation ^{31}P-MRI sequence shown in Fig. 4B[25]. Acquisition parameters of the sequence are summarized in Table 2. In both the ST spectroscopy and imaging acquisitions, we used a ST module consisting of a train of Gaussian pulses (each 50 ms long, with 56 Hz bandwidth and 0.85 μT strength at peak), which saturates the γ-ATP resonance. Between two consecutive pulses a 7 ms delay allows for the use of spoiler gradients (magnitude 20 mT m^{-1}; duration 5 ms) to destroy any remaining transverse magnetization. The number of Gaussian pulses defines t_{sat} in each experiment.

The imaging sequence was a centric ordered three-dimensional turbo spin echo (3D-TSE) with a frequency selective 90° pulse (16 ms duration, 125 Hz bandwidth) that excited only the PCr resonance[25]. The effective echo was 26 ms, which resulted in minimum contamination from ATP signal[26]. A train of 24 non-selective 180° pulses was applied after each excitation, using equal area crusher gradients to remove the free inductions decays (FIDs) that were produced by imperfections of the refocusing pulses. During the ST imaging experiments, the SAR levels never exceeded 5% of the maximum allowed under normal operating mode.

This k-space sampling scheme resulted in increased blurring in the imaging direction where the ETL was sampled. We simulated the effect of signal modulation during the ETL acquisition in order to predict the point-spread-function (PSF) along that direction, using an average T_2 value of PCr of 365 ms based on previous measurements[11] which were in close agreement with T_2 values at 3.0 T reported in the literature[24].

Table 2 | Acquisition parameters of the reference (t_{sat} = 0) and ST ^{31}P-MRS and ^{31}P-MRI data

	^{31}P-MRS		^{31}P-MRI	
	Reference	ST	Reference	ST
Exciation Pulse (ms)	0.2	0.2	16	16
TR (s)	20	15	20	15
Number of acquisitions	1	5	1	8
t_{sat} (s)	0	0.57, 1.14 1.71 3.42, 6.84	0	0.57, 1.14, 1.71, 2.56, 4.43, 4.27, 5.13, 6.84
Effective echo time (ms)	NA	NA	26	26
Echo spacing (ms)	NA	NA	26	26
Echo train length	NA	NA	24	24
FID Sampling points	2048	2048	NA	NA
Field of view (mm^3)	Entire coil	Entire coil	220 × 220 × 200	220 × 220 × 200
Matrix size	NA	NA	48 × 48 × 8	48 × 48 × 8
Resolution (mm^3)	Entire coil	Entire coil	4.6 × 4.6 × 25	4.6 × 4.6 × 25
Voxel Size (mL)	Entire coil	Entire coil	0.5	0.5
Acquistion time (min:sec)	0:20	1:15	5:20	32:00

Note: FID = free induction decay, NA = not applicable.

For absolute quantification of PCr in the muscle we imaged a phantom with comparable to the in vivo coil loading, using the same ^{31}P-MRI sequence and parameters (with the ST module turned off), with the exception of repetition time (TR) of 60 s. We used the phantom to derive the calibration curve of PCr as a function of signal intensity. The phantom consisted of three sealed cylindrical tubes containing different concentrations (25, 50 and 75 mM) of inorganic phosphate (Pi).

^{1}H Water-Fat Imaging. Fat infiltration, especially in high BMI subjects, can reduce the volume fraction of lean muscle in a certain volume of tissue affecting quantification of PCr concentration. In order to account for the fat content in the muscle, we used a three-dimensional gradient echo sequence with three echo-times (TE: 2.1, 2.8 and 3.7 ms; flip angle: 3°; TR: 12 ms, total acquisition time: 3 min), with the same FOV and frame of reference as the PCr images. The matrix size was 128 × 128 × 40. We reconstructed water and fat fraction images using the Hierarchical IDEAL method[15] on all ten healthy volunteers. These fractions represent the proton density fat and water fractions and can be converted to volume fat and water fractions as shown previously[27].

Data Analysis. For each muscle group, we estimated k_f from Eq.2 by fitting the mean signal intensity of the segmented PCr datasets at different t_{sat} (excluding slices 1 and 8 at the edge of the coil). We estimated V_f from the product of k_f and PCr concentration in the same volume of the muscle. We compared k_f and V_f values among four different muscle groups [Gastrocnemius Lateralis (GL) and Medialis (GM), Soleus (S), and Tibialis Anterior (TA)], with paired t-tests with a 5% significance level.

1. Ingwall, J. S. Is cardiac-failute a consequence of decreased energy reserve? *Circulation* **87**, 58–62 (1993).
2. Radda, G. K. The use of NMR spectroscopy for the understanding of disease. *Science* **233**, 640–645 (1986).
3. Jennings, R. B. & Reimer, K. A. Lethal myocardial ischemic-injury. *Am. J. Pathol.* **102**, 241–255 (1981).
4. Alger, J. R. & Shulman, R. G. NMR-studies of enzymatic rates in vitro and in vivo by magnetization transfer. *Q. Rev. Biophys.* **17**, 83–124 (1984).
5. Ingwall, J. S. *et al.* The creatine kinase system in normal and diseased human myocardium. *N. Engl. J. Med.* **313**, 1050–1054 (1985).
6. Bottomley, P. A. *et al.* Metabolic Rates of ATP Transfer Through Creatine Kinase (CK Flux) Predict Clinical Heart Failure Events and Death. *Sci. Transl. Med.* **5**, 215re213 (2013).
7. Valkovič, L. *et al.* Time-resolved phosphorous magnetization transfer of the human calf muscle at 3 T and 7 T: A feasibility study. *Eur. J. Radiol.* **82**, 745–751 (2013).
8. Schar, M., El-Sharkawy, A.-M. M., Weiss, R. G. & Bottomley, P. A. Triple Repetition Time Saturation Transfer (TRiST) (31)P Spectroscopy for Measuring Human Creatine Kinase Reaction Kinetics. *Magn. Reson. Med.* **63**, 1493–1501 (2010).
9. Lu, A., Atkinson, I. C., Zhou, X. J. & Thulborn, K. R. PCr/ATP ratio mapping of the human head by simultaneously imaging of multiple spectral Peaks with interleaved excitations and flexible twisted projection imaging readout trajectories at 9.4 T. *Magn. Reson. Med.* **69**, 538–544 (2013).
10. Steinseifer, I. K., Wijnen, J. P., Hamans, B. C., Heerschap, A. & Scheenen, T. W. Metabolic imaging of multiple X-nucleus resonances. *Magn. Reson. Med.* **70**, 169–175 (2013).
11. Parasoglou, P., Xia, D., Chang, G. & Regatte, R. R. 3D-Mapping of Phosphocreatine Concentration in the Human Calf Muscle at 7T: Comparison to 3T. *Magn. Reson. Med.* **70**, 1616–1625 (2013).
12. Kraff, O., Fischer, A., Nagel, A. M., Mönninghoff, C. & Ladd, M. E. MRI at 7 tesla and above: Demonstrated and potential capabilities. *J. Magn. Resonan. Imag.* doi: 10.1001/jmri.24573 (2014).
13. Forsen, S. & Hoffman, R. A. Study of moderately rapid chemical exchange reactions by means of nuclear magnetic double resonance. *J. Chem. Phys.* **39**, 2892–2901 (1963).
14. Horska, A. & Spencer, R. G. S. Correctly accounting for radiofrequency spillover in saturation transfer experiments: Application to measurement of the creatine kinase reaction rate in human forearm muscle. *MAGMA* **5**, 159–163 (1997).
15. Tsao, J. & Jiang, Y. Hierarchical IDEAL: Fast, robust, and multiresolution separation of multiple chemical species from multiple echo times. *Magn. Reson. Med.* **70**, 155–150 (2012).
16. Kholmovski, E. G., Parker, D. L. & Alexander, A. L. A generalized k-sampling scheme for 3D fast spin echo. *J. Magn. Resonan. Imag.* **11**, 549–558 (2000).
17. Gabr, R. E., Weiss, R. G. & Bottomley, P. A. Correcting reaction rates measured by saturation-transfer magnetic resonance spectroscopy. *J. Magn. Reson.* **191**, 248–258 (2008).
18. Suzuki, E. *et al.* H-1- and P-31-magnetic resonance spectroscopy and imaging as a new diagnostic tool to evaluate neuropathic foot ulcers in Type II diabetic patients. *Diabetologia* **43**, 165–172 (2000).
19. Bottomley, P. A. & Hardy, C. J. Mapping creatine kinase reaction rates in human brain and heart with 4 tesla saturation transfer 31P NMR. *J. Magn. Reson.* **99**, 443–448 (1992).
20. Bottomley, P. A., Ouwerkerk, R., Lee, R. F. & Weiss, R. G. Four-angle saturation transfer (FAST) method for measuring creatine kinase reaction rates in vivo. *Magn. Reson. Med.* **47**, 850–863 (2002).
21. Kemp, G. J., Meyerspeer, M. & Moser, E. Absolute quantification of phosphorus metabolite concentrations in human muscle in vivo by P-31 MRS: a quantitative review. *NMR Biomed.* **20**, 555–565 (2007).
22. Parasoglou, P., Xia, D., Chang, G., Convit, A. & Regatte, R. R. Three-dimensional mapping of the creatine kinase enzyme reaction rate in muscles of the lower leg. *NMR Biomed.* **26**, 1142–1151 (2013).
23. Jeong, E.-K. *et al.* Measurement of creatine kinase reaction rate in human brain using magnetization transfer image-selected in vivo spectroscopy (MT-ISIS) and a volume P-31/H-1 radiofrequency coil in a clinical 3-T MRI system. *NMR Biomed.* **24**, 765–770 (2011).
24. Bogner, W. *et al.* Assessment of (31)P Relaxation Times in the Human Calf Muscle: A Comparison between 3 T and 7 T In Vivo. *Magn. Reson. Med.* **62**, 574–582 (2009).
25. Parasoglou, P., Xia, D. & Regatte, R. R. Spectrally selective 3D TSE imaging of phosphocreatine in the human calf muscle at 3 T. *Magn. Reson. Med.* **69**, 812–817 (2013).
26. Chao, H., Bowers, J. L., Holtzman, D. & Mulkern, R. V. Multi-echo 31P spectroscopic imaging of ATP: A scan time reduction strategy. *J. Magn. Resonan. Imag.* **7**, 425–433 (1997).
27. Hu, H. H., Li, Y., Nagy, T. R., Goran, M. I. & Nayak, K. S. Quantification of absolute fat mass by magnetic resonance imaging: a validation study against chemical analysis. *Int. J. Body Compos. Res.* **9**, 111 (2011).

Acknowledgments

The research was supported by the National Institute of Arthritis and Musculoskeletal and Skin Diseases (NIAMS) of the National Institutes of Health (NIH) (grants K23 AR059748, RO1 AR056260 and RO1 AR060238).

Author contributions

P.P. and R.R.R. designed the experiment. P.P., D.X., G.C. and R.R.R. coordinated/performed the experiments analyzed the data. P.P., D.X., G.C. and R.R.R. interpreted the results. All authors contributed to the final manuscript.

Additional information

Competing financial interests: The authors declare no competing financial interests.

How to cite this article: Parasoglou, P., Xia, D., Chang, G. & Regatte, R.R. Three-dimensional Saturation Transfer ^{31}P-MRI in Muscles of the Lower Leg at 3.0 T. *Sci. Rep.* **4**, 5219; DOI:10.1038/srep05219 (2014).